Atmospheric Science Letters

RMetS Royal Meteorological Society

RESEARCH ARTICLE OPEN ACCESS

Statistical Characteristics of Dabie-Vortex-Associated Tornadogenesis During an 18-Year Period (2006–2023)

Xue Xiao[1,2] | Shen-Ming Fu[1,3] | Yuan-Chun Zhang[3,4] | Jing-Ping Zhang[5] | Jian-Hua Sun[6] | Xaio Li[7] | You Dong[8] | Shu-Guang Ning[9] | Shi-Jun Sun[9]

[1]State Key Laboratory of Earth System Numerical Modeling and Application, Institute of Atmospheric Physics, Chinese Academy of Sciences, Beijing, China | [2]University of Chinese Academy of Sciences, Beijing, China | [3]China Meteorological Administration Tornado Key Laboratory, Guangzhou, Guangdong, China | [4]State Key Laboratory of Atmospheric Environment and Extreme Meteorology, Institute of Atmospheric Physics, Chinese Academy of Sciences, Beijing, China | [5]Beijing School, Beijing, China | [6]Key Laboratory of Cloud-Precipitation Physics and Severe Storms, Institute of Atmospheric Physics, Chinese Academy of Sciences, Beijing, China | [7]School of Civil Engineering, Chongqing University, Chongqing, China | [8]Department of Civil and Environmental Engineering, The Hong Kong Polytechnic University, Hong Kong, China | [9]Shandong Electric Power Meteorological Technology Innovation Center, Shandong Luruan Digital Technology Co. Ltd, Jinan, Shandong Province, China

Correspondence: Shen-Ming Fu (fusm@mail.iap.ac.cn)

Received: 16 May 2025 | **Revised:** 17 August 2025 | **Accepted:** 15 September 2025

Funding: This work was supported by Science and Technology Foundation of State Grid Corporation of China, 5200-202415102A-1-1-ZN.

Keywords: convection | Dabie vortex | mesoscale vortices | tornado | tropical cyclone

ABSTRACT

The Dabie vortex (DBV), a mesoscale system frequently generating severe weather in the Yangtze River Basin, exhibits spatial overlap with tornado-prone regions, yet its tornadic potential remains unexplored. This study identifies 23 tornadoes associated with DBV occurring between 2006 and 2023, primarily concentrated in the provinces of Jiangsu, Anhui, Hubei, and Henan. In northern Anhui, DBVs contribute up to 40% of tornadoes—surpassing Jiangsu (~29%) and rivaling half the frequency of tropical cyclone (TC)-induced events. Approximately 70% of tornadoes occur in the DBV's southeastern quadrant, favored by enhanced CAPE, low-level moisture, vertical wind shear, and storm-relative helicity. Most (87%) form during DBV development/maintenance phases, when dynamical forcing peaks. Compared to TC tornadoes, DBV tornadoes exhibit stronger instability and vertical wind shear. Relative to other-type tornadoes, they develop in environments with weaker instability but greater moisture, stronger shear, and greater storm-relative helicity. These findings underscore DBVs as a previously overlooked but critical driver of tornado activity in eastern China.

1 | Introduction

Per the American Meteorological Society Glossary (2025), a tornado is a violently rotating column of air extending vertically from the earth's surface to the base of a cumuliform cloud. Due to its extremely strong winds, tornadoes are one of the most destructive natural phenomena, causing massive social and ecological consequences (Antonescu et al. 2017; Púčik et al. 2024; Li et al. 2024). Consequently, tornado research has remained an enduring scientific priority in both meteorological science and disaster risk reduction sectors.

Given their typically small horizontal scale (< 2 km; Markowski and Richardson 2010), tornadoes are inherently difficult to detect and forecast directly. Consequently, research has long focused on (i) deciphering the convective environments conducive to tornadogenesis, and (ii) developing operational forecasting metrics to assess tornado potential. For instance, vertical

wind shear is a critical driver for tornadogenesis as it converts horizontal vorticity to vertical vorticity, which is essential for mesocyclone development (Davies-Jones 1984; Droegemeier et al. 1993; Fischer et al. 2024). The magnitude of shear can distinguish between significant and weak tornado events (Dupilka and Reuter 2006; Púčik et al. 2015; Reames 2017), and it can modulate the frequency and spatial distribution of tornadoes in tropical cyclones (Schenkel et al. 2020, 2021). Regional differences in tornado environments also exist, with U.S. tornadoes driven by strong dynamic forcing, while Chinese tornadoes are characterized by weaker shear and are humidity driven (Zhang, Xue, et al. 2023; Zhou et al. 2022). Other important metrics include storm-relative helicity (SRH; Davies-Jones et al. 1990) and composite parameters, including the Supercell Composite Parameter (SCP) and Significant Tornado Parameter (STP), both introduced by Thompson et al. (2003).

As tornadogenesis-favorable convective conditions are usually created within specific synoptic-scale environments, research has extensively examined the connections between tornadoes and the synoptic-scale weather systems that generate these conditions. In the United States, tornadoes are frequently linked to upper-level troughs, extratropical cyclones (ECs), and jet stream dynamics (McCaul 1991; Bray et al. 2021; Jiang et al. 2025), whereas in Japan, tornado development is more commonly attributed to ECs and typhoons (Fujiwara et al. 2024). Specifically, ECs can trigger tornado outbreaks primarily through their distinct structure and induced environments (Li et al. 2022). For example, meridionally elongated ECs often produce strong low-level southerly jets and cold fronts, transporting warm, moist air, enhancing SRH, CAPE, and energy-helicity index (EHI). Meanwhile, these ECs are located near upper-level jet exits, further supporting convective development (Tochimoto and Niino 2016).

In China, which borders Siberia to the north, high-latitude cold vortices (i.e., the northeast cold vortex) are active in late spring and early summer, creating favorable conditions for severe convection by promoting the interaction of cold and warm, moist air. Previous studies have found that tornadoes frequently occur in the southeastern and southwestern quadrants of intensifying northeast cold vortices (Cai et al. 2022; Wang et al. 2022). Along the southeastern coast of China facing the vast Northwest Pacific Ocean, typhoons frequently make landfall in summer, providing ideal conditions for tornadic supercells due to strong low-level wind shear and low lifting condensation levels (Yao et al. 2019; Bai 2021). Approximately one-third of landfalling tropical cyclones in China can spawn tornadoes, with the highest probability in the northeastern quadrant of the typhoon circulation (Bai et al. 2020). Tornadogenesis can also be modulated by mesoscale terrain-coastline interactions (Bai, Yao, Meng, Zhang, et al. 2024, 2024) and frequent frontal activities, such as those within the mei-yu front system (Zhang et al. 2016; Wang and Min 2023; Li et al. 2024). Mesoscale vortices embedded within the mei-yu front can enhance vertical wind shear and low-level convergence, further supporting the formation of tornadic supercells (Wang and Min 2023).

While previous studies have documented tornadoes under large-scale systems such as ECs, northeast cold vortices, typhoons, and mei-yu fronts, little attention has been paid to the possible tornadic influence of smaller-scale vortices such as the Dabie Vortex (DBV; Fu et al. 2016; Zhang et al. 2015). The DBV, typically forming over the middle and lower reaches of the Yangtze River Basin with a horizontal scale of 100–400 km, is most prominent at 850 hPa and is often associated with heavy rainfall and extreme precipitation events (Dong 2011; Fu et al. 2025; Yang et al. 2010). Previous studies (Fan and Yu 2015; Fu et al. 2016, 2025; Chen et al. 2018) have established central and eastern China as a hotspot for both tornadogenesis and Dabie Vortex (DBV) activity. While DBVs are known to create favorable conditions for severe convective weather, including heavy precipitation and lightning, their potential relationship with tornadoes remains unexplored. Targeting this knowledge gap, this study aims to address three key scientific questions: (i) What statistical linkages exist between DBVs and tornadogenesis? (ii) What are the primary characteristics of tornadoes occurring amid DBV environments? (iii) How do DBV-associated tornadoes differ from those formed under non-DBV conditions? Addressing these questions will advance our fundamental understanding of tornadogenesis while offering critical insights for operational tornado forecasting in China.

The reminder of the article is structured as follows: Section 2 shows the data and methods; Section 3 presents characteristics of tornadoes within DBV contexts; Section 4 discusses the differences in background conditions between DBV-related tornadoes and those from other systems; and a conclusion is reached in Section 5.

2 | Data and Methods

2.1 | Data

This study uses three datasets: (i) The DBV dataset, which is generated through an objective identification algorithm developed by Zhang, Jin, et al. (2023) and validated through rigorous manual quality control. Spanning 45 warm seasons (1979–2023) with hourly resolution, this dataset documents DBV centers, vertical extent, and formation/dissipation times (Fu et al. 2025). (ii) The tornado dataset (2006–2023) is provided by the China Meteorological Administration Tornado Key Laboratory. It includes tornadoes' exact times and locations, synoptic backgrounds (tropical cyclones, Northeast China cold vortices). It should be noted that other important background circulations (e.g., ECs, frontal zones, and low-level jets) are absent from the dataset's classification, despite evidence for their role in tornadogenesis. Particularly, tornadoes spawned by thunderstorms within 1000 km of a tropical cyclone's center are classified as tropical cyclone tornadoes (TC tornadoes). (iii) The atmospheric reanalysis data from the fifth-generation European Centre for Medium-Range Weather Forecasts (ERA5), featuring 0.25° spatial resolution and hourly temporal resolution. While ERA5 may underestimate certain parameters, it is considered a reliable source for studying convective environments (Taszarek et al. 2021; Hanesiak et al. 2024).

2.2 | Selection of Tornadoes Under DBV Background

To select tornadoes under DBV background, we follow these steps: (i) Influence range determining: we average the wind

TABLE 1 | Definitions of the environmental parameters analyzed in this study.

Parameter	Abbreviation	Definition	Unit
Most unstable CAPE	MUCAPE	CAPE computed from the most buoyant air parcel between the surface and 300 hPa, representing the maximum convective potential.	$J kg^{-1}$
Mixed-layer CAPE	MLCAPE	CAPE calculated by averaging temperature and moisture over the lowest 100 hPa from the surface, reflecting mean boundary-layer instability.	$J kg^{-1}$
Surface-based CAPE	SBCAPE	CAPE based on a surface parcel, sensitive to near-surface heating and moisture content.	$J kg^{-1}$
Lifted condensation level	LCL	The height at which an air parcel becomes saturated when lifted dry adiabatically from the surface.	m
0–1 (3) km vertical wind shear	VWS1 (3)	The vector difference in wind between the surface and 1/3 km above ground level, indicating lower-tropospheric shear.	$m s^{-1}$
0–1/3 km storm-relative helicity	SRH1 (3)	A measure of streamwise vorticity in the storm inflow layer (0–3/6 km), related to updraft rotation potential.	$m^2 s^{-2}$
Supercell composite parameter	SCP	A composite index combining MLCAPE, SRH3, and VWS6 to estimate the potential for supercell development.	—
Significant tornado parameter	STP	A composite index incorporating MLCAPE, VWS6, SRH3, and LCL height to estimate the likelihood of EF2+ tornadoes.	—

fields at DBV-occurring moments to obtain the DBV composite circulation pattern from 2006 to 2023. Based on this pattern, we define the DBV influence range as a circle with a radius of 3.5° (~350 km) around the vortex center. (ii) Temporal aligning: In our classification scheme, any tornado occurring within a 60-min window (±30 min) centered on a DBV detection time is considered potentially DBV-related. (iii) Spatiotemporal matching: Tornadoes meeting the temporal criteria (ii) are classified as DBV-associated (hereinafter referred to as DBV tornadoes) if they occur within a 3.5° radius of DBV centers during the vortex lifespan (from formation to dissipation).

2.3 | Calculation of the Relative Time

To determine the life stage of DBV during which the tornadoes occur, the relative time (T_R) is calculated as:

$$T_R = \frac{T_{TND} - T_{DBVf}}{T_{DBVd} - T_{DBVf}} \quad (1)$$

where T_{TND} is the tornado's occurrence time, while T_{DBVf} and T_{DBVd} are the formation and dissipation times of DBV, respectively. DBVs' life cycles are classified into three equal stages: development ($0 < T_R \leq \frac{1}{3}$), maintenance ($\frac{1}{3} < T_R \leq \frac{2}{3}$), and dissipation ($\frac{2}{3} < T_R \leq 1$) stages.

2.4 | Convection Parameters

To compare environmental conditions between tornadoes under DBV and non-DBV backgrounds, we calculate convection and tornadic parameters using ERA5 data at the nearest 0.25° grid point and the nearest hourly time preceding each tornado event. The definitions and abbreviations of the environmental parameters analyzed in this study are summarized in Table 1. All parameters are calculated using Metpy functions (May et al. 2022) after interpolating 37-layer ERA5 data to surface pressure levels and removing sub-surface data.

3 | Characteristics of Tornadoes Amid DBV Background

3.1 | Spatial Distribution

During 2006–2023, a total of 775 tornadoes were recorded within the regions historically affected by DBVs (Figure 1a), with the highest frequencies in eastern and southern China, particularly Jiangsu and Guangdong provinces. Of the 720 DBVs identified in the same period, 11 (~1.5%) DBVs were associated with 23 tornado events (~3.0% of the total). These DBV tornadoes showed clear geographical clustering: 17 cases in Jiangsu (~9.3% of all tornadoes in the province), with additional occurrences in Anhui, Hubei, and Henan (Figure 1b). As shown in Figure 1c, the contribution of DBV tornadoes to the total tornado count within each 1°×1° grid peaks in Anhui at approximately 40%, which is notably higher than the ~33% in Henan and Hubei and ~29% in Jiangsu. Within the region outlined by the red contour in Figure 1, where the DBV appearance frequency exceeds 500 (i.e., the total number of DBV occurrences per 0.25°×0.25° grid cell during 1979–2020; based on Fu et al. 2025), the contribution reaches ~5.0%. The study highlights the underappreciated role of DBVs, as Jiangsu, a high-frequency tornado province, recorded 17 DBV-related tornadoes compared to 27 TC-associated ones.

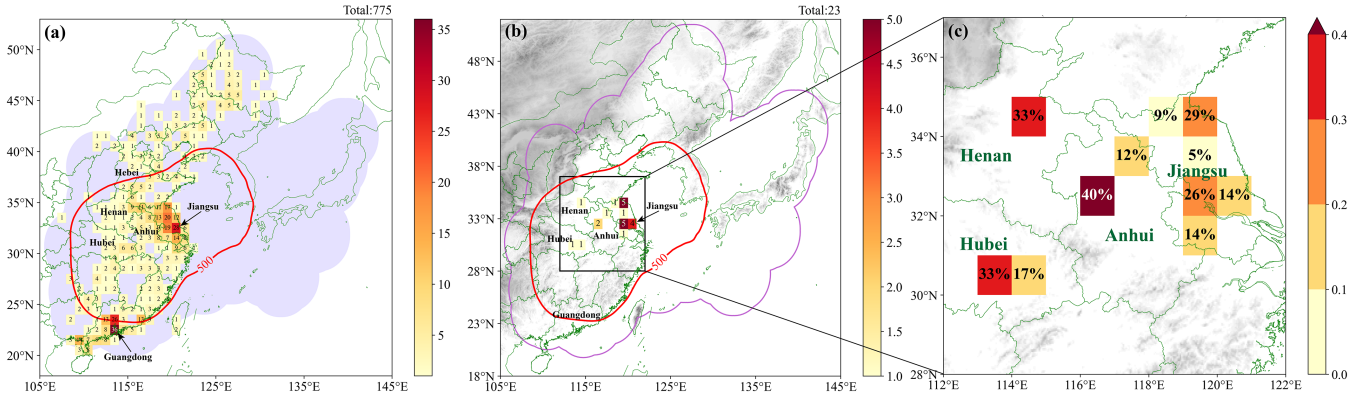

FIGURE 1 | Panel (a) shows the distribution of tornadoes from 2006 to 2023, where numbers represent the tornado count in each 1°×1° grid cell. The purple shading indicates the historically influence range of DBVs. The red line outlines the region with DBV's appearance frequency ≥500, defined as the number of DBV occurrences per 0.25°×0.25° grid cell during 1979–2020, following Fu et al. (2025). Panel (b) shows the distribution of DBV tornadoes, with the purple contours representing the DBV's influence range. Panel (c) represents the contribution of DBV tornadoes to the total number of tornadoes in each grid cell.

Historically, DBVs have been understudied and not separately classified in tornado statistics, which has contributed to a limited awareness of their role in tornadogenesis.

3.2 | Quadrant Distribution

According to Fu et al. (2016), DBVs possess distinct quadrant-dependent properties that ultimately determine how tornadoes are spatially distributed relative to the vortices. As evident from Figure 3, DBV tornadoes predominantly cluster in the southeastern (SE) quadrant, accounting for ~69.6% of occurrences. The northeastern (NE) and southwestern (SW) quadrants contribute ~21.7% and ~8.7%, respectively, with these tornadoes all located near the SE quadrant boundary (Figure 3a). Notably, no tornadoes are documented in the northwestern (NW) quadrant. This pronounced spatial distribution highlights the SE quadrant as the main area for tornadogenesis under DBV conditions.

To understand this distinct spatial distribution of tornadoes, we examine the horizontal distribution of convective parameters (Section 2.4). Figure 2 presents composite fields of circulation and environmental parameters at the hourly times preceding tornado occurrence. While thermodynamic parameters such as MUCAPE, MLCAPE, SBCAPE, and LCL (Figure 2a–d) show limited spatial correspondence with tornado locations, dynamic parameters like VWS1, SRH1, and SCP (Figure 2e–g) are more consistently aligned with the tornado occurrences. These findings underscore that low-level dynamic forcing, including wind shear and helicity, may be more reliable indicators of tornadogenesis than thermodynamic instability in these cases.

Further comparison between the SE and NW quadrants revealed striking environmental contrasts. The SE quadrant had significantly higher CAPE values (approximately 1071.8–1913.5 J kg^{-1}; Figures 3b–d) and a lower median LCL (~392.4 m) compared to the NW quadrant, which had minimal CAPE (0.4–73.0 J kg^{-1}) and a higher LCL (~654.5 m; Figure 3e). Dynamic parameters are also markedly stronger in the SE quadrant, with stronger VWS1/VWS3 (median of ~9.5 and 13.5 m s^{-1}) than in the NW quadrant (median of ~2.8 and 5.6 m s^{-1}; Figure 3f–g), suggesting an environment favorable for sustaining storm and upward tilting of horizontal vorticity near the surface. Storm-relative helicity also exhibits striking contrasts, with SRH3 in the SE quadrant (median: ~129.9 m^2 s^{-2}) being nearly an order of magnitude greater than in the NW quadrant (median: ~14.0 m^2 s^{-2}; Figure 3i). SRH1 displays an even more dramatic contrast with positive values in the SE quadrant (median: ~90.4 m^2 s^{-2}) contrasting sharply with negative values in the NW quadrant (median: ~−7.2 m^2 s^{-2}; Figure 3h), indicating superior storm-relative wind shear alignment that enhances tornadic supercell potential in the SE quadrant. The SE quadrant also showed significantly higher supercell and tornadic parameters (median SCP: ~3.1; STP: ~0.3) compared to the negligible values in the NW quadrant (Figure 3j–k). These combined thermodynamic and dynamic differences fundamentally explain why tornadogenesis predominantly occurs in the SE quadrant.

3.3 | Relations With the Dbvs' Life Stages

DBV tornadoes occur across all lifecycle stages of the vortex, with ~86.9% (20 of 23 events) concentrated during the development and maintenance stages (Figure 4a). Only three tornadoes form during the dissipation stage. Notably, DBVs are more productive (producing multiple tornadoes per vortex) during their earlier lifecycle stages, as the development-stage tornadoes involved four distinct DBVs, while the three dissipation-stage tornadoes originated from only two DBVs.

Given the concentration of DBV tornadoes during the development and maintenance stages, we examined potential stage-dependent environmental differences. Tornadoes during the development stage exhibit lower median energy values (MLCAPE: ~864.2 J kg^{-1}; SBCAPE: ~694.8 J kg^{-1}) than maintenance-stage events (MLCAPE: ~1329.2 J kg^{-1}; SBCAPE: ~2264.6 J kg^{-1}; Figure 4c,d). MUCAPE values are also shown in Figure 4b, but differences among the three lifecycle stages are not statistically significant at the 95% confidence level. Contrary to expectations, this suggests maintenance-stage tornadoes

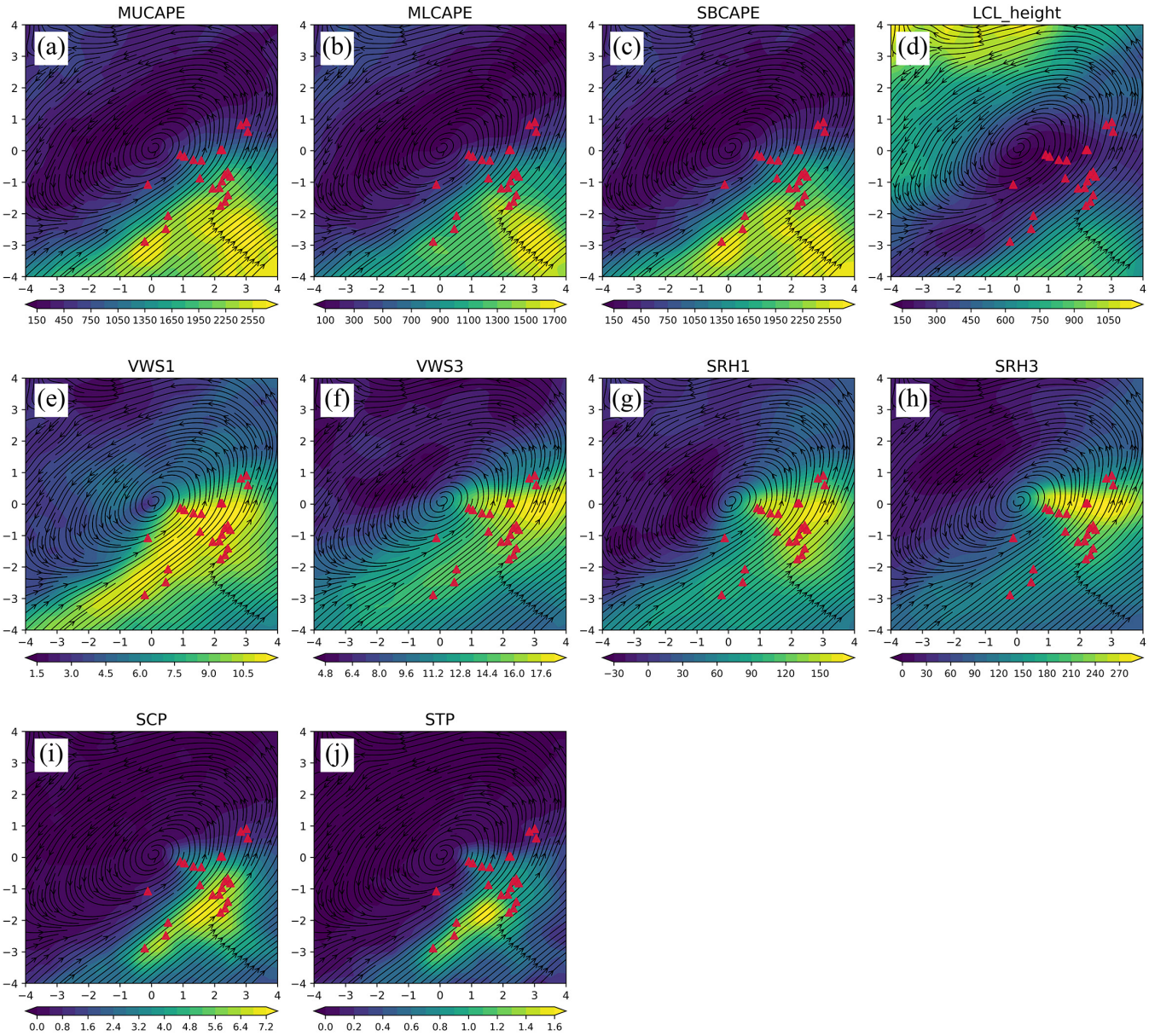

FIGURE 2 | Horizontal distributions of composite environmental parameters associated with DBV tornadoes. Panels (a–c) display show MUCAPE, MLCAPE and SBCAPE, all in $J\,kg^{-1}$. Panels (d) shows LCL height (m). Panels (e) and (f) depict show 0–1 km and 0–3 km vertical wind shear (VWS; $m\,s^{-1}$), while panels (g) and (h) illustrate 0–1 km and 0–3 km storm-relative helicity (SRH; $m^2\,s^{-2}$). Panels (i–j) show SCP and STP, both unitless. Tornado locations are marked with a red triangle.

develop under stronger SBCAPE and MLCAPE, despite their later occurrence in the DBV lifecycle. The development stage exhibits a substantially lower median LCL height (~197.9 m) compared to both the maintenance (~392.4 m) and dissipation stages (~486.1 m; Figure 4e), indicating optimal low-level moisture availability and reduced convective inhibition during initial DBV evolution.

Analyses of vertical wind shear show that the development stage exhibits significantly stronger VWS3 (median of ~19.0 $m\,s^{-1}$) compared to maintenance (~14.2 $m\,s^{-1}$) and dissipation stages (~13.7 $m\,s^{-1}$; Figure 4g). Similarly, VWS1 in the development stage (~13.3 $m\,s^{-1}$) exceeds dissipation-stage values (~7.9 $m\,s^{-1}$; Figure 4f). Storm-relative helicity analysis reveals substantially enhanced vortex support during development stages, with median SRH1 (~154.4 $m^2\,s^{-2}$) and SRH3 (~244.6 $m^2\,s^{-2}$) values approximately double those observed during dissipation (~81.0 and ~149.8 $m^2\,s^{-2}$, respectively; Figure 4h,i). In contrast, SCP and STP remain statistically invariant across lifecycle stages (Figure 4j,k), suggesting consistent potential for tornadic intensity regardless of DBV maturity. These analyses show that dynamical conditions peak during DBV development, creating optimal tornadogenesis environments that degrade during dissipation.

In summary, stage-controlled tornadogenesis mechanisms emerge: Development-stage events leverage strong dynamical forcing and moist boundary layers, while dissipation-stage tornadoes rely primarily on residual instability amid weakening kinematic support.

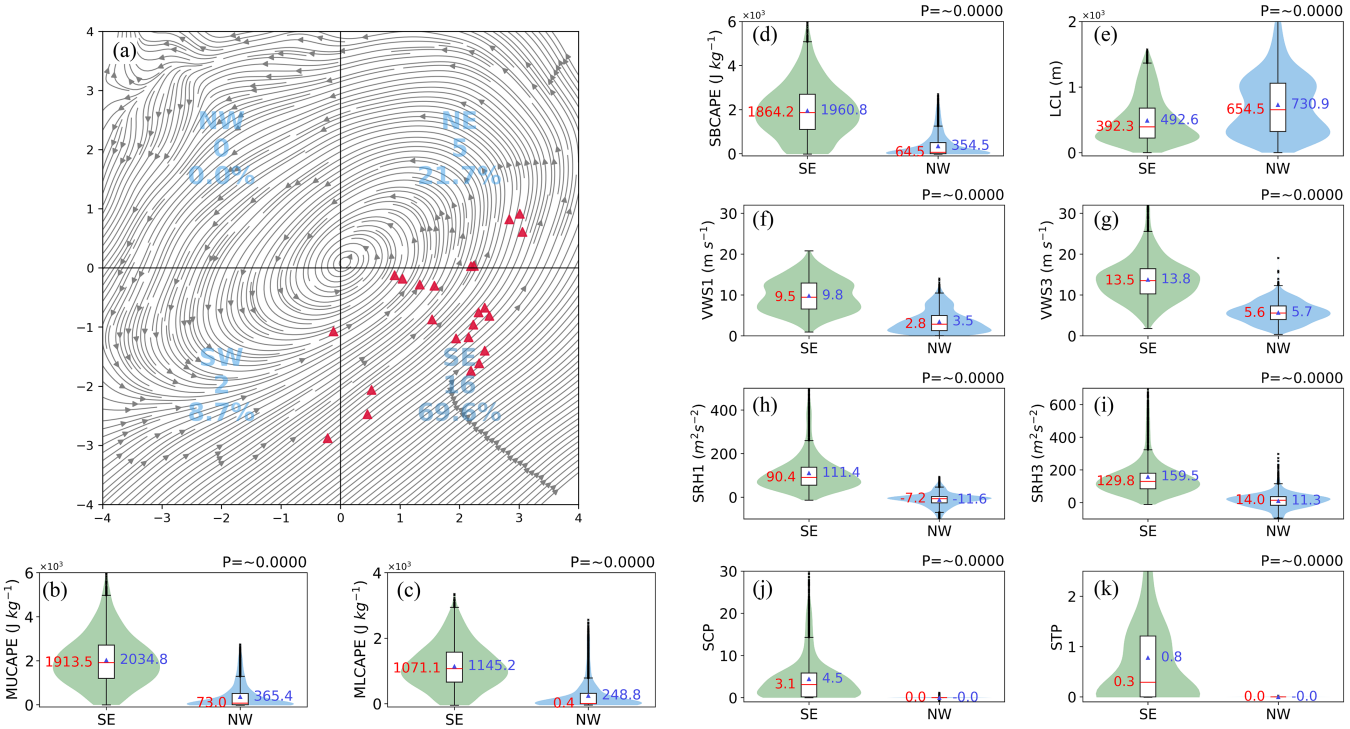

FIGURE 3 | Panel (a) presents the composite 850 hPa circulation at the time of tornado occurrence, centered on the DBV. The x- and y-axes represent longitude and latitude relative to the DBV center. Red triangles indicate tornado locations. Blue numbers indicate the count and percentage of tornadoes. Panels (b–k) compare convection parameters on 0.25° grids in the SE and NW quadrants at tornado occurrence times, where violin plots display kernel density estimates, red lines and numbers represent median values, and blue triangles and numbers show mean values. All the parameters pass the 99% significance T-test.

4 | Contrast Tornadoes Under Different Backgrounds

Given that both DBVs and TCs serve as critical background conditions for tornado formation in Jiangsu, Anhui, Hubei, and Henan (Section 3.1), we compare the convective environments conducive to tornadogenesis under different systems, including DBV, TCs, and other synoptic backgrounds (abbreviated as 'Other'). The comparison includes 23 cases of DBV tornadoes, 27 cases of TC tornadoes, and 179 cases of other-type tornadoes, with parameters calculated using the methodology outlined in Section 2.4.

DBVs and TCs exhibit fundamentally different structures. DBVs are shallow, meso-α-scale systems triggered by low-level jets and upper-level shortwave troughs over the Yangtze Basin (Fu et al. 2013, 2017; Zhang et al. 2015). In contrast, TCs are deep, synoptic systems driven by oceanic latent heat release under weak vertical wind shear and warm sea surfaces. Despite these contrasts, both systems share certain common features. For instance, DBVs are often accompanied by a low-level jet and strong convergence, which can enhance moisture transport and vertical wind shear. Similarly, tropical cyclones also exhibit strong moisture transport capability due to their intense cyclonic circulation and sustained low-level inflow that continuously channels moist air from the ocean.

Compared to TC environments, DBV tornadoes demonstrate significantly enhanced CAPE values, with median MUCAPE, MLCAPE, and SBCAPE values (~1882.5, ~999.1, and ~1825.9 J kg^{-1} respectively; Figure 5a–c). This pronounced difference in convective energy occurs despite comparable LCL heights between the two systems (Figure 5d), revealing that while DBV tornadoes develop within environments of greater convective potential, their low-level moisture characteristics remain similar to TC cases. Vertical wind shear is also stronger in DBV environments, with a median VWS3 of ~16.0 m s^{-1} (Figure 5f) compared to ~12.9 m s^{-1} for TC tornadoes. Remarkably, the minimum VWS3 values for DBV tornadoes approximate the 25th percentiles of TC cases, highlighting more consistently favorable shear conditions. While SRH1/SRH3 shows no statistically significant variation (Figure 5g,h), DBV environments have greater supercell potential, as evidenced by significantly higher median SCP values (~4.8 versus ~2.1 for TC cases; Figure 5i), though STP distributions show no meaningful inter-regime differences (Figure 5j).

DBV tornadoes also have characteristics that distinguish them from other-type tornadoes. While other-type tornadoes have higher median MLCAPE and SBCAPE values (~1605.6 and 2277.8 J kg^{-1}; Figure 5b,c), DBV tornadoes have a lower LCL height (~327.2 m; Figure 5d). This indicates that DBV tornadoes form in environments with less convective energy but more low-level moisture. Regarding dynamic parameters, DBV tornadoes show stronger vertical wind shear (median VWS1 and VWS3 of ~12.0 and ~17.0 m s^{-1}) than other-type tornadoes (~5.7 and ~10.1 m s^{-1}; Figure 5e,f). DBV tornadoes also show stronger storm-relative helicity (Figure 5g,h). For composite parameters, DBV tornadoes exhibit markedly higher SCP and STP values (while those for other-type tornadoes approach zero;

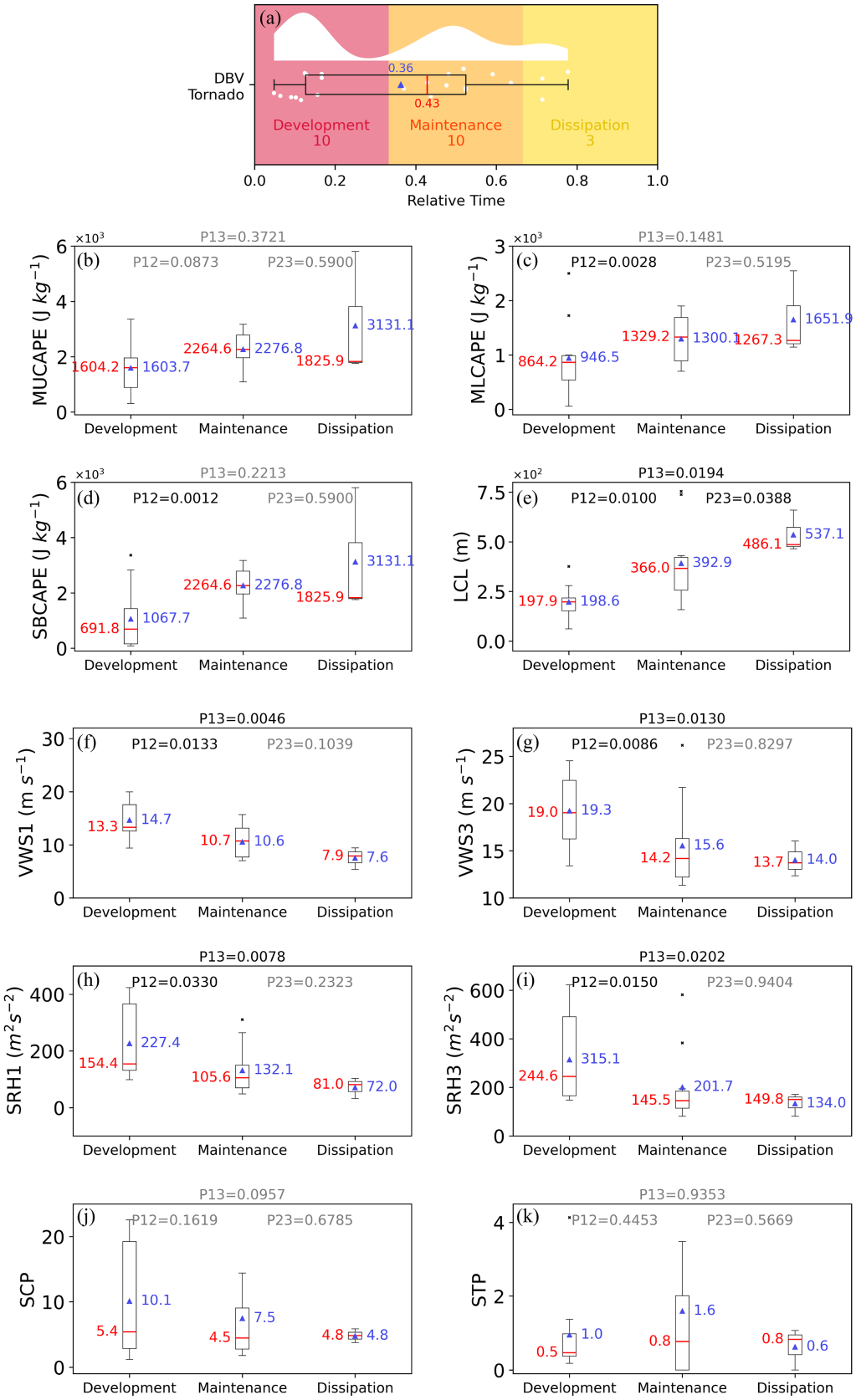

FIGURE 4 | Panel (a) shows the relative occurrence times of tornadoes (calculated as described in Section 2.3). The half-violin plot represents the probability density distribution of DBV tornadoes, while white dots denote individual tornado samples. The blue triangle and red vertical line indicate the mean and median values, respectively. The numbers below the stage labels indicate the tornado count in each stage. Panel (b–k) presents convection parameters of tornadoes occurring in three life cycle stages of DBVs. The red lines and red numbers represent the medians, while the blue triangles and blue numbers represent the means. Pij denotes the P-value of the T-test between the i-th and j-th boxplots. Black Pij indicates that the result passes the 95% significance test, and gray Pij indicates non-significance.

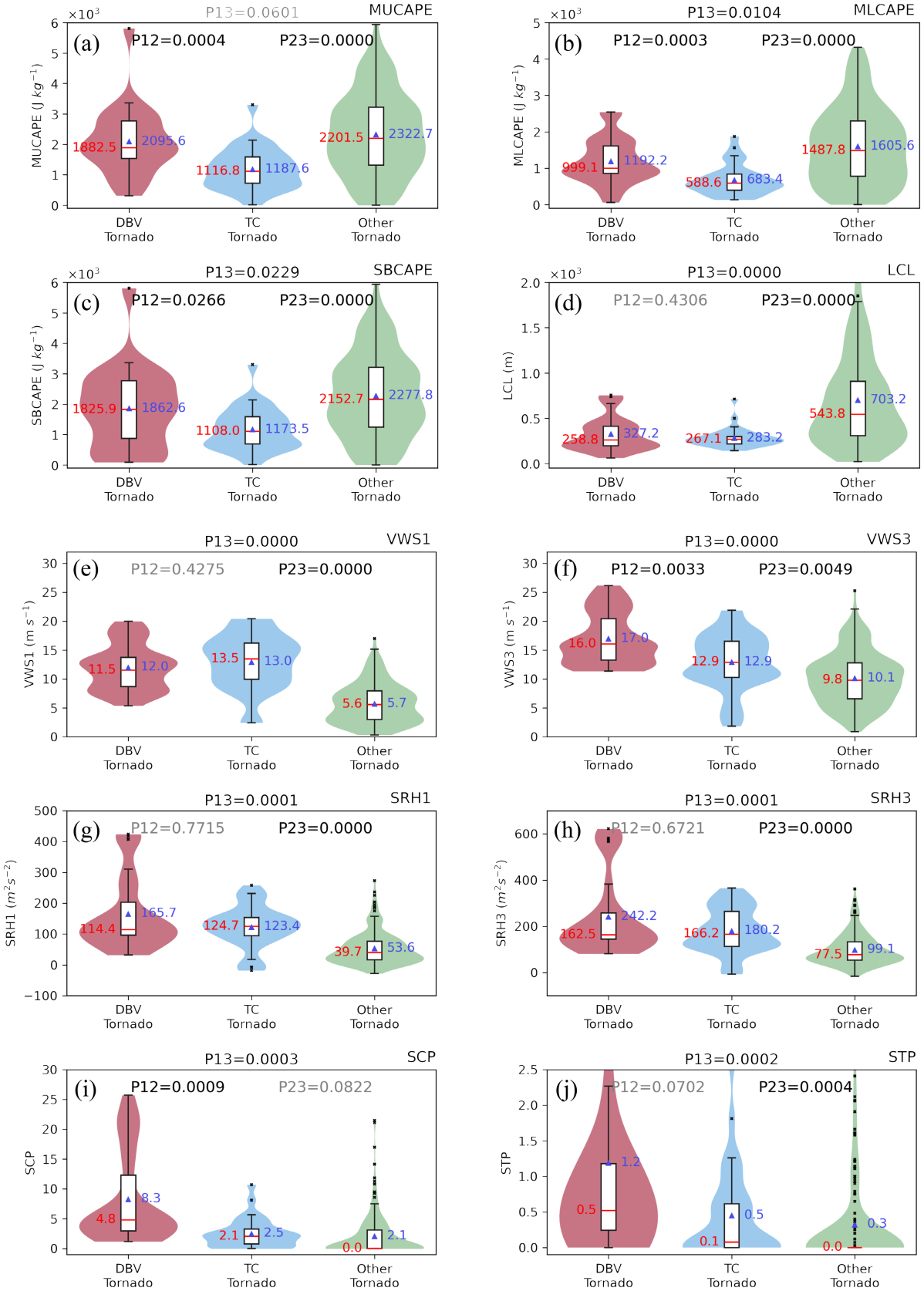

FIGURE 5 | Convection parameters of tornadoes under DBV, TC and Other type backgrounds, where violin plots display kernel density estimates, red lines and numbers represent median values, and blue triangles and numbers show mean values. Pij denotes the P-value of the T-test between the i-th and j-th boxplots. Black Pij indicates that the result passes the 95% significance test, and gray Pij indicates non-significance.

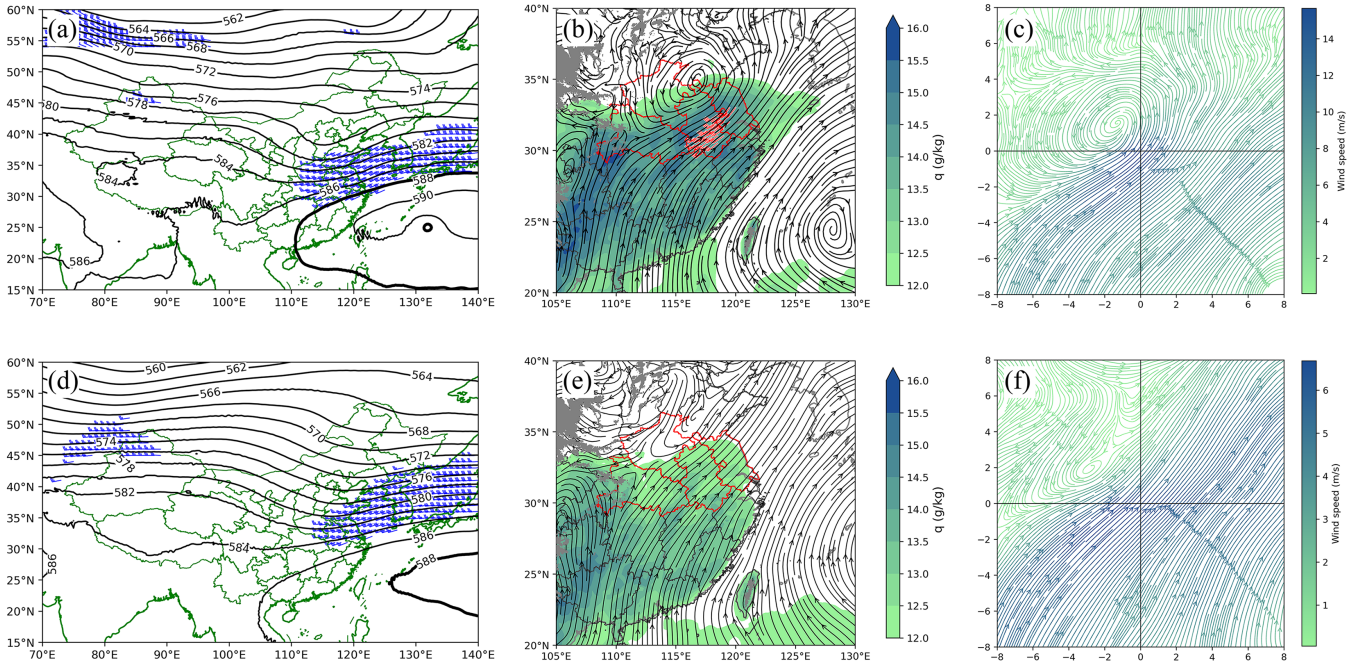

FIGURE 6 | Composite circulation patterns for DBV tornadoes (a–c) and other-type tornadoes (d–f). Panels (a) and (d) show 500 hPa circulation, with contours representing geopotential height (unit: gpm) and wind barbs indicating winds ≥ 10 m s^{-1}. The 588-gpm contour denotes the position of the subtropical high. Panels (b) and (e) show the 850-hPa circulation, with shading indicating absolute humidity (unit: g kg^{-1}) and wind barbs indicating winds ≥ 12 m s^{-1}. Red boundaries enclose provinces where DBV tornadoes have been documented. Panels (c) and (f) show the composite 850 hPa circulation centered on the tornado location, with (0, 0) denoting the tornado center; streamline colors indicate wind speed (unit: M s^{-1}).

Figure 5h,i), indicating more favorable environments for supercell organization and intense tornadogenesis. Overall, DBV tornadoes occur in an environment with more abundant water vapor and better dynamic conditions but with slightly less unstable energy.

Possible reason for these differences appears to be related to the synoptic-scale circulation. Both types of tornadoes typically occur ahead of a 500 hPa trough (Figure 6a,d). However, for DBV tornado cases, the subtropical high is positioned farther west (Figure 6a). At 850 hPa, the subtropical high is also farther west, with a low-level jet present between the DBV and the subtropical high (Figure 6b). In contrast, for other-type tornadoes, the subtropical high is farther east (Figure 6e), and there is a low system (like a cut-off low), with weaker absolute humidity and no low-level jet. The tornado-centered composites (Figure 6c,f) indicate that both DBV and other-type tornadoes occur on the southeastern flank of a cyclonic circulation. However, for DBV cases, this cyclone is larger, more circular, and closer to the tornadoes. Furthermore, the southwesterly flow in DBV environments exceeds 14 m s^{-1}, whereas in other-type tornado cases it is around 6 m s^{-1}. These differences suggest that a low-level jet between the DBV and the subtropical high may play a key role in enhancing the conditions for DBV tornado formation.

In summary, DBV tornado environments offer distinct advantages over TC cases, featuring stronger convective instability, more pronounced VWS, and greater supercell potential, highlighting fundamental differences in their tornadogenesis-supporting environments. Compared with other types of tornadoes, DBV tornadoes form in environments with weaker instability but greater low-level moisture, markedly stronger VWS, greater SRH, and higher SCP/STP values. These more favorable conditions are related to the synoptic circulation, as DBV tornadoes are often associated with a westward-shifted subtropical high and a pronounced low-level jet. This synoptic setup enhances low-level moisture transport and vertical wind shear.

5 | Conclusions and Discussions

This study establishes crucial distinctions between tornado environments associated with DBVs, TCs, and other-type systems through analysis of 775 tornado events (2006–2023) using ERA5 reanalysis and data from the China Meteorological Administration Tornado Key Laboratory. Results show DBV tornadoes (23 cases) predominantly cluster in Jiangsu, Anhui, Hubei, and Henan provinces, accounting for 40% of northern Anhui's tornadoes and over 25% in Jiangsu, with DBVs contributing half the tornadic potential of TCs in Jiangsu. Spatial analysis reveals ~69.6% of DBV tornadoes form in the SE quadrant, contrasting with TC tornadoes' northeastern quadrant preference, driven by superior environmental conditions in DBV's SE quadrant: higher convection energy, lower LCLs, stronger VWS1/VWS3, enhanced SRH1/SRH3, and elevated supercell potential compared to non-tornadic NW quadrants. These stem from intense southwesterly moisture transport into DBVs' SE quadrants (Fu et al. 2025), while TC tornadoes concentrate in northeastern quadrants due to maximal shallow-layer shear (Schultz and Cecil 2009; Bai et al. 2020; Deng et al. 2024). Temporally, ~86.9% of DBV tornadoes occur during development/maintenance phases, with development-stage tornadoes exhibiting stronger dynamics and lower LCLs than dissipation-stage cases. Comparative analysis shows DBV

tornado environments surpass TC cases in convection energy, vertical shear, and supercell potential, though sharing comparable LCLs and SRH. Compared with other-type tornadoes, DBV tornadoes form in environments with weaker instability but greater low-level moisture, markedly stronger VWS, greater SRH, and higher SCP/STP values.

The results highlight distinct tornadogenesis mechanisms in DBV environments that fundamentally differ from both TC and other-type systems. This comprehensive analysis significantly advances our understanding of midlatitude vortex-driven tornadogenesis by quantitatively establishing the specific environmental characteristics favoring tornado development under each synoptic regime, thereby providing critical baseline data for improving operational forecasting of East Asian severe storms, though the inherent limitations of ERA5 reanalysis data in resolving convective-scale processes must be carefully considered when interpreting these findings.

Author Contributions

Xue Xiao: software, data curation, investigation, formal analysis, visualization, writing – original draft. **Shen-Ming Fu:** conceptualization, methodology, validation, supervision, funding acquisition, project administration, writing – review and editing, resources, investigation. **Yuan-Chun Zhang:** supervision, validation, resources, investigation. **Jing-Ping Zhang:** investigation, data curation, software. **Jian-Hua Sun:** supervision, validation, resources, investigation. **Xaio Li:** project administration, resources, investigation. **You Dong:** investigation, project administration, resources. **Shu-Guang Ning:** project administration, resources, investigation. **Shi-Jun Sun:** project administration, resources, investigation.

Acknowledgments

This work was supported by the Science and Technology Foundation of State Grid Corporation of China (Grant 5200-202415102A-1-1-ZN). The authors thank ECMWF for providing the ERA5 data. Special thanks are given to CMA Tornado Key Laboratory for providing the tornado data. The authors would like to thank the anonymous reviewers for their valuable comments.

Conflicts of Interest

The authors declare no conflicts of interest.

Data Availability Statement

The ERA5 data used in this study (Hersbach et al. 2020) are freely available on Copernicus Data Store at https://doi.org/10.24381/cds.bd0915c6. The tornado dataset used in this study is publicly available at the China Tornado Database (https://www.fs121.com/tornado/#/list?code=11100).

References

American Meteorological Society. 2025. "Tornado. Glossary of Meteorology." http://glossary.ametsoc.org/wiki/Tornado.

Antonescu, B., D. M. Schultz, A. Holzer, and P. Groenemeijer. 2017. "Tornadoes in Europe: An Underestimated Threat." *Bulletin of the American Meteorological Society* 98, no. 4: 713–728. https://doi.org/10.1175/BAMS-D-16-0171.1.

Bai, L.-Q. 2021. "Environmental Analysis on the First Documented Tornado Outbreak in China." *Atmospheric Science Letters* 22, no. 10: e1057. https://doi.org/10.1002/asl.1057.

Bai, L.-Q., Z.-Y. Meng, K. Sueki, G.-X. Chen, and R.-L. Zhou. 2020. "Climatology of Tropical Cyclone Tornadoes in China From 2006 to 2018." *Science China Earth Sciences* 63, no. 1: 37–51. https://doi.org/10.1007/s11430-019-9391-1.

Bai, L.-Q., D. Yao, Z. Meng, Y. Zhang, X.-X. Huang, and Z.-M. Li. 2024. "Influence of Irregular Coastlines on a Tornadic Mesovortex in the Pearl River Delta During Monsoon Season. Part II: Numerical Experiments." *Advances in Atmospheric Sciences* 41, no. 9: 1704–1720. https://doi.org/10.1007/s00376-023-3096-4.

Bai, L.-Q., D. Yao, Z.-Y. Meng, et al. 2024. "Influence of Irregular Coastlines on a Tornadic Mesovortex in the Pearl River Delta During the Monsoon Season. Part I: Pre-Storm Environment and Storm Evolution." *Advances in Atmospheric Sciences* 41, no. 6: 1115–1131. https://doi.org/10.1007/s00376-023-3095-5.

Bray, M. T., S. M. Cavallo, and H. B. Bluestein. 2021. "Examining the Relationship Between Tropopause Polar Vortices and Tornado Outbreaks." *Weather and Forecasting* 36, no. 5: 1799–1814. https://doi.org/10.1175/WAF-D-21-0058.1.

Cai, K.-Z., X.-P. Yao, X.-W. Sun, and P. Cheng. 2022. "Climatic Characteristics and Environmental Conditions of Tornadoes in Liaoning Under the Background of Cold Vortex (In Chinese)." *Acta Meteorologica Sinica* 80, no. 1: 82–92. https://doi.org/10.11676/qxxb2021.063.

Chen, J.-Y., X.-H. Cai, H. Wang, et al. 2018. "Tornado Climatology of China." *International Journal of Climatology* 38, no. 5: 2478–2489. https://doi.org/10.1002/joc.5369.

Davies-Jones, R., D. W. Burgess, and M. Foster. 1990. "Test of Helicity as a Forecast Parameter (pp. 588–592)." In *Presented at the 16th Conference on Severe Local Storms*. American Meteorological Society.

Davies-Jones, R. 1984. "Streamwise Vorticity: The Origin of Updraft Rotation in Supercell Storms." *Journal of the Atmospheric Sciences* 41, no. 20: 2991–3006. https://doi.org/10.1175/1520-0469(1984)041<2991:SVTOOU>2.0.CO;2.

Deng, Y.-X., T.-G. Xiao, Z.-Y. Tang, Z. Shi, and L.-Y. Xiao. 2024. "Statistical Analysis of Tornado Activity and Environmental Characteristics Under the Influence of Tropical Cyclones in Jiangsu and Anhui Area From 2007 to 2021 (In Chinese)." *Journal of the Meteorological Sciences* 44, no. 4: 663–672. https://doi.org/10.12306/2023jms.0019.

Dong, Q.-S. 2011. *Characteristics of Warm Season Mesoscale Vortices Over theMiddle and Lower Reaches of Yangtze River.* Nanjing University.

Droegemeier, K. K., S. M. Lazarus, and R. Davies-Jones. 1993. "The Influence of Helicity on Numerically Simulated Convective Storms." *Monthly Weather Review* 121, no. 7: 2005–2029. https://doi.org/10.1175/1520-0493(1993)121<2005:TIOHON>2.0.CO;2.

Dupilka, M. L., and G. W. Reuter. 2006. "Forecasting Tornadic Thunderstorm Potential in Alberta Using Environmental Sounding Data. Part I: Wind Shear and Buoyancy." *Weather and Forecasting* 21, no. 3: 325–335. https://doi.org/10.1175/WAF921.1.

Fan, W. -J., and X. -D. Yu. 2015. "Characteristics of Spatial Temporal Distribution of Tornadoes in China (In Chinese)." *Meteorological Monthly* 41, no. 7: 793–805.

Fischer, J., J. M. L. Dahl, B. E. Coffer, et al. 2024. "Supercell Tornadogenesis: Recent Progress in Our State of Understanding." *Bulletin of the American Meteorological Society* 105, no. 7: E1084–E1097. https://doi.org/10.1175/BAMS-D-23-0031.1.

Fu, S.-M., J.-H. Sun, J. Ling, H.-J. Wang, and Y.-C. Zhang. 2016. "Scale Interactions in Sustaining Persistent Torrential Rainfall Events During the Mei-Yu Season." *Journal of Geophysical Research: Atmospheres* 121, no. 21: 12,856–12,876. https://doi.org/10.1002/2016JD025446.

Fu, S.-M., J.-H. Sun, Y.-L. Luo, and Y.-C. Zhang. 2017. "Formation of Long-Lived Summertime Mesoscale Vortices Over Central East China: Semi-Idealized Simulations Based on a 14-Year Vortex Statistic." *Journal of the Atmospheric Sciences* 74, no. 12: 3955–3979. https://doi.org/10.1175/JAS-D-16-0328.1.

Fu, S.-M., F. Yu, D.-H. Wang, and R.-D. Xia. 2013. "A Comparison of Two Kinds of Eastward-Moving Mesoscale Vortices During the Mei-Yu Period of 2010." *Science China Earth Sciences* 56, no. 2: 282–300. https://doi.org/10.1007/s11430-012-4420-5.

Fu, S.-M., J.-P. Zhang, X. Xiao, T.-T. Huang, and J.-H. Sun. 2025. "A 42-Years Statistic on the Dabie Vortices: Multi-Scale Temporal Characteristics and Associated Mechanisms, and Hourly-Rainfall Features." *Journal of Climate* 38, no. 7: 1553–1572. https://doi.org/10.1175/JCLI-D-24-0304.1.

Fujiwara, K., D. Nohara, Y. Eguchi, Y. Hattori, and H. Hirakuchi. 2024. "Impact of Synoptic Weather Patterns Along the Pacific Coastline of Japan on Tornado Wind Hazard Curves." Proceedings of the 31st International Conference on Nuclear Engineering (ICONE31), Volume 10: Risk Assessments and Management; Computer Code Verification and Validation; Nuclear Education and Public Acceptance, American Society of Mechanical Engineers, Paper No. V010T12A009, 8 pp. https://doi.org/10.1115/ICONE31-135030.

Hanesiak, J., M. Taszarek, D. Walker, C.-C. Wang, and D. Betancourt. 2024. "ERA5-Based Significant Tornado Environments in Canada Between 1980 and 2020." *Journal of Geophysical Research: Atmospheres* 129, no. 8: e2023JD040614. https://doi.org/10.1029/2023JD040614.

Hersbach, H., B. Bell, P. Berrisford, et al. 2020. "The ERA5 Global Reanalysis." *Quarterly Journal of the Royal Meteorological Society* 146, no. 730: 1999–2049. https://doi.org/10.1002/qj.3803.

Jiang, Q., D. T. Dawson, F. -N. Li, and D. R. Chavas. 2025. "Classifying Synoptic Patterns Driving Tornadic Storms and Associated Spatial Trends in the United States." *npj Climate and Atmospheric Science* 8, no. 1: 1–10. https://doi.org/10.1038/s41612-025-00897-1.

Li, C., L.-Q. Bai, X.-D. Yu, et al. 2022. "A Brief Discussion on the High-Impact Cold-Season Tornado Outbreak During 10-11 December 2021 in the United States." *Journal of Tropical Meteorology* 28, no. 2: 252–260. https://doi.org/10.46267/j.1006-8775.2022.019.

Li, Y., S.-Y. Cao, X.-H. Wang, and L. Wang. 2024. "Comparative Analysis of Two Tornado Processes in Southern Jiangsu." *Atmosphere* 15, no. 8: 1010. https://doi.org/10.3390/atmos15081010.

Markowski, P., and Y. Richardson. 2010. *Mesoscale Meteorology in Midlatitudes*. Wiley-Blackwell.

May, R. M., K. H. Goebbert, J. E. Thielen, et al. 2022. "MetPy: A Meteorological Python Library for Data Analysis and Visualization." *Bulletin of the American Meteorological Society* 103, no. 10: E2273–E2284. https://doi.org/10.1175/BAMS-D-21-0125.1.

McCaul, E. W. 1991. "Buoyancy and Shear Characteristics of Hurricane-Tornado Environments." *Monthly Weather Review* 119, no. 8: 1954–1978. https://doi.org/10.1175/1520-0493(1991)119<1954:BASCOH>2.0.CO;2.

Púčik, T., P. Groenemeijer, D. Rýva, and M. Kolář. 2015. "Proximity Soundings of Severe and Nonsevere Thunderstorms in Central Europe." *Monthly Weather Review* 143, no. 12: 4805–4821. https://doi.org/10.1175/MWR-D-15-0104.1.

Púčik, T., D. Rýva, M. Staněk, et al. 2024. "The Violent Tornado on 24 June 2021 in Czechia: Damage Survey, Societal Impacts, and Lessons Learned." *Weather, Climate, and Society* 16, no. 3: 411–429. https://doi.org/10.1175/WCAS-D-23-0080.1.

Reames, L. J. 2017. "Diurnal Variations in Severe Weather Forecast Parameters of Rapid Update Cycle-2 Tornado Proximity Environments." *Weather and Forecasting* 32, no. 2: 743–761. https://doi.org/10.1175/WAF-D-16-0029.1.

Schenkel, B. A., M. Coniglio, and R. Edwards. 2021. "How Does the Relationship Between Ambient Deep-Tropospheric Vertical Wind Shear and Tropical Cyclone Tornadoes Change Between Coastal and Inland Environments?" *Weather and Forecasting* 36, no. 2: 539–566. https://doi.org/10.1175/WAF-D-20-0127.1.

Schenkel, B. A., R. Edwards, and M. Coniglio. 2020. "A Climatological Analysis of Ambient Deep-Tropospheric Vertical Wind Shear Impacts Upon Tornadoes in Tropical Cyclones." *Weather and Forecasting* 35, no. 5: 2033–2059. https://doi.org/10.1175/WAF-D-19-0220.1.

Schultz, L. A., and D. J. Cecil. 2009. "Tropical Cyclone Tornadoes, 1950–2007." *Monthly Weather Review* 137, no. 10: 3471–3484. https://doi.org/10.1175/2009MWR2896.1.

Taszarek, M., N. Pilguj, J. T. Allen, V. Gensini, H. E. Brooks, and P. Szuster. 2021. "Comparison of Convective Parameters Derived From ERA5 and MERRA-2 With Rawinsonde Data Over Europe and North America." *Journal of Climate* 34, no. 8: 3211–3237. https://doi.org/10.1175/JCLI-D-20-0484.1.

Thompson, R. L., R. Edwards, J. A. Hart, K. L. Elmore, and P. Markowski. 2003. "Close Proximity Soundings Within Supercell Environments Obtained From the Rapid Update Cycle." *Weather and Forecasting* 18, no. 6: 1243–1261. https://doi.org/10.1175/1520-0434(2003)018<1243:CPSWSE>2.0.CO;2.

Tochimoto, E., and H. Niino. 2016. "Structural and Environmental Characteristics of Extratropical Cyclones That Cause Tornado Outbreaks in the Warm Sector: A Composite Study." *Monthly Weather Review* 144, no. 3: 945–969. https://doi.org/10.1175/MWR-D-15-0015.1.

Wang, S.-Q., and J.-Z. Min. 2023. "Dynamical Analyses of a Supercell Tornado in Eastern China Based on a Real-Data Simulation." *Atmosphere* 14, no. 5: 884. https://doi.org/10.3390/atmos14050884.

Wang, Y.-P., T. Wang, P. Yang, and W. Xue. 2022. "A Numerical Simulation of the "1907" Kaiyuan Tornado Weather Process in Liaoning, Northeast China." *Atmosphere* 13, no. 2: 219. https://doi.org/10.3390/atmos13020219.

Yang, Y.-M., W.-L. Gu, R.-L. Zhao, and J. Liu. 2010. "The Statistical Analysis of Low Vortex During Meiyu Season in the Lower Reaches of the Yangtze (In Chinese)." *Journal of Applied Meteorological Science* 21, no. 1: 11–18.

Yao, D., X.-D. Liang, Q. Meng, et al. 2019. "Importance of Identifying Tropical Cyclone Tornadoes in Typhoon Warning and Defense Systems." *Science Bulletin* 64, no. 3: 143–145. https://doi.org/10.1016/j.scib.2018.12.022.

Zhang, C.-Y., M. Xue, K.-F. Zhu, and X.-D. Yu. 2023. "Climatology of Significant Tornadoes Within China and Comparison of Tornado Environments Between the United States and China." *Monthly Weather Review* 151, no. 2: 465–484. https://doi.org/10.1175/MWR-D-22-0070.1.

Zhang, J.-P., S.-M. Fu, X.-Y. Shen, and Y.-C. Zhang. 2015. "A Statistical and Compositional Study on the Two Types of Mesoscale Vortices Over the Yangtze River Basin (In Chinese)." *Climatic and Environmental Research* 20, no. 3: 319–336. https://doi.org/10.3878/j.issn.1006-9585.2015.14164.

Zhang, J.-P., S.-L. Jin, S.-L. Feng, H. Han, and S.-M. Fu. 2023. "A New Objective Identification Method for Mesoscale Vortices: Three-Dimensional Tracking and Quantitative Evaluation." *Chinese Journal of Atmospheric Sciences* 47, no. 5: 1434–1450. https://doi.org/10.3878/j.issn.1006-9895.2111.21178.

Zhang, X.-L., B. Yang, W.-J. Zhu, et al. 2016. "Analysis of the EF4 Tornado in Funing County, Jiangsu Province on 23 June 2016 (In Chinese)." *Meteorological Monthly* 42, no. 11: 1304–1314.

Zhou, R.-L., Z.-Y. Meng, and L.-Q. Bai. 2022. "Differences in Tornado Activities and Key Tornadic Environments Between China and the United States." *International Journal of Climatology* 42, no. 1: 367–384. https://doi.org/10.1002/joc.7248.